Solar RRL
www.solar-rrl.com

22.6% Efficient Solar Cells with Polysilicon Passivating Contacts on n-type Solar-Grade Wafers

Rabin Basnet, Sieu Pheng Phang, Christian Samundsett, Di Yan, Wensheng Liang, Chang Sun, Stephane Armand, Roland Einhaus, Julien Degoulange, and Daniel Macdonald*

Czochralski (Cz)-grown upgraded metallurgical-grade (UMG) silicon wafers degrade significantly during high-temperature processes, eroding their appeal as a low-cost alternative to conventional electronic-grade silicon wafers. However, the thermal degradation in UMG wafers can be delayed by utilizing a prefabrication annealing step. Based on this, a high-efficiency solar-cell process is modified by selecting a single-boron diffusion step and applying phosphorus-doped polycrystalline films as electron-selective contacts with excellent impurity-gettering properties to minimize the thermal budget. The application of this modified high-efficiency solar-cell process to n-type UMG-Cz wafers results in a solar cell with a conversion efficiency of 22.6% on a cell area of $2 \times 2\,cm^2$.

1. Introduction

Upgraded metallurgical-grade (UMG) silicon is a promising low-cost solar-grade feedstock material for silicon solar cells. With improved purification methods, recent work has demonstrated that solar cells based on UMG wafers can achieve efficiencies above 21%.[1–4] However, UMG feedstock materials still have relatively high concentrations of metallic (e.g., Fe, Cu, and Cr) and nonmetallic impurities (e.g., C and O) compared with electronic-grade wafers purified via the Siemens process. As a result, UMG wafers are susceptible to high-temperature degradation.[5] A prefabrication annealing step known as a tabula rasa (TR) can help to mitigate high-temperature degradation[6–8] on n-type Czochralski (Cz)-grown UMG wafers, by dissolving the grown-in oxygen precipitate nuclei, which can otherwise become recombination-active during processing, appearing as ring defects.[5] Furthermore, phosphorus diffusion gettering is a powerful method to remove mobile impurities.[9,10] Hence, utilizing appropriate prefabrication treatments, solar-grade wafers can potentially be suitable for high-efficiency solar cells.[11]

Recently, the advent of passivating contacts based on ultrathin silicon oxide (SiO_x) films with overlaid doped polysilicon layers has enabled very high efficiencies to be achieved.[12–14] This approach combines outstanding surface passivation with excellent carrier-selective electrical contact and allows full-area rear-side passivation, thus avoiding the need for patterning steps, in contrast to some other high-efficiency structures, such as passivated emitter and rear locally diffused (PERL) cells.[4,15] In addition, these doped-polycrystalline films have been shown to provide strong impurity-gettering effects,[16,17] which can replace the standard phosphorus diffusion gettering, and therefore is attractive for applications to low-cost substrates such as UMG or cast silicon wafers.

In this article, we have developed a modified high-efficiency solar-cell process, including a TR preanneal and a full-area phosphorus-doped polysilicon contacts on the rear-side and applied it to n-type UMG-Cz wafers. The adapted solar cell process is designed to minimize the thermal budget to avoid the activation of oxygen precipitates and take full advantage of the excellent gettering effects provided by the polysilicon structure, which is formed by plasma-enhanced chemical vapor deposited (PECVD) intrinsic amorphous silicon films that are subsequently doped and crystallized by phosphorus diffusion.[14,18]

2. Experimental Section

The compensated n-type UMG-Cz wafers were supplied by Apollon Solar in the framework of the PHOTOSIL.[19] The phosphorus, boron, and carbon concentrations in the UMG-Cz were measured by secondary-ion mass spectrometry (SIMS), and for the selected UMG-Cz wafers, these concentrations were calculated by fitting Scheil's equation,[20] using the effective segregation coefficients of 0.8 and 0.35[21] for boron and phosphorus and 0.3 for carbon.[22] The selected UMG wafers had a boron concentration $[B] = 1.3 \times 10^{16}\,cm^{-3}$ and a phosphorus concentration $[P] = 1.7 \times 10^{16}\,cm^{-3}$, and a

R. Basnet, Dr. S. P. Phang, C. Samundsett, Dr. D. Yan, Dr. W. Liang, Dr. C. Sun, S. Armand, Prof. D. Macdonald
Research School of Electrical
Energy and Materials Engineering
The Australian National University
Canberra, ACT 2601, Australia
E-mail: rabin.basnet@anu.edu.au

Dr. R. Einhaus, Dr. J. Degoulange
Apollon Solar
Multiparc Parilly, Batiment D2, 50, Rue Jean Zay, 69800 Saint-Priest, France

The ORCID identification number(s) for the author(s) of this article can be found under https://doi.org/10.1002/solr.201900297.

DOI: 10.1002/solr.201900297

carbon concentration $[C] = 1.0 \times 10^{16}\,cm^{-3}$. The interstitial oxygen concentrations $[O_i] = 6.3 \times 10^{17}\,cm^{-3}$ were measured by Fourier-transform infrared spectroscopy (FTIR) (Bruker Vertex 80) and were calibrated using SEMI MF standard 1188-1107. Electronic-grade n-type float-zone (FZ) wafers were used as controls and had a doping concentration of $n_0 = [P] = 2.3 \times 10^{15}\,cm^{-3}$, as determined by dark conductance measurements.

For cell fabrication convenience, 4-inch round UMG wafers were laser cut from the 6-inch pseudosquare wafers. Lifetime samples were prepared by dicing 6-inch wafers into four quarters. All samples were saw-damage-etched in tetramethylammonium hydroxide (TMAH) solution to remove 10–12 μm from each side, with final thicknesses of 150 and 280 μm for the UMG and FZ wafers, respectively. Samples were cleaned using standard radio corporation of America (RCA) cleaning steps prior to each high-temperature step. The TR step in this work was optimized for the UMG-Cz wafers[5] and performed in oxygen at 1000 °C for 30 min with loading and unloading temperatures at 700 °C and ramp up and down rates of 15 °C min^{-1}. A stack of ≈10 nm thermal SiO_x and 70 nm low-pressure chemical vapor-deposited (LPCVD) silicon nitride (Si_3N_4) was used as a diffusion mask. The thermal SiO_x was grown in oxygen at 888 °C for 1 min with loading and unloading temperatures at 700 °C and ramp up and down rates of 15 °C min^{-1}. The LPCVD SiN_x layer was deposited at 775 °C for 15 min. The solar cells of $2 \times 2\,cm^2$ size were defined on the front surface through the diffusion mask using photolithography.

To assess the impact of the thermal budget, solar cells with double-boron diffusion (DBD) for a selective emitter and single-boron diffusion (SBD) for a homogenous emitter were fabricated. For the DBD process, a deep and heavy boron diffusion was performed at 850 °C for 30 min using boron tribromide (BBr_3), with an additional drive-in at 955 °C for 60 min, followed by a 20 min post-oxidation, resulting in a sheet resistance of $R_{sheet} = 45\,\Omega/\square^{-1}$. The diffusion mask was then removed, and the front grid was defined through a masking layer using photolithography. The boron-diffused regions between the fingers were etched back, and random pyramids were formed using TMAH and a wetting agent (RENA monoTEX). Subsequently, a lighter boron diffusion was performed at 930 °C for 35 min, followed by a post-oxidation at 930 °C for 40 min, resulting in $R_{sheet} = 180\,\Omega/\square^{-1}$. For the SBD process, the samples were textured, and a full-area boron diffusion was performed at 930 °C for 20 min deposition with an additional 25 min post-oxidation followed by a 20 min drive-in to achieve $R_{sheet} = 130$–$140\,\Omega/\square^{-1}$.

After the front-side diffusions, a fresh diffusion mask was deposited, and the rear-side mask was removed by concentrated hydrofluoric acid (HF) fuming. An ultrathin SiO_x (≈1.4 nm) layer was grown in boiling nitric acid, and subsequently, intrinsic amorphous silicon layers (≈50 nm) were overlaid using PECVD (Roth & Rau AK400). The amorphous silicon layers were then phosphorus doped using phosphorus oxychloride as dopant source at 820 °C for 25 min and a drive-in for 30 min with further details in previous study.[14]

AlO_x/SiN_x stacks deposited by atomic layer deposition (Benq TFS200) and PECVD were used for front antireflection and surface passivation, respectively. Then, the front metal grid was defined by photolithography and a Cr/Pd/Ag stack was evaporated and lifted-off. Then, the rear metal contact was formed by evaporating a uniform 600 nm thick layer of silver, and cells were subjected to silver electroplating to thicken the finger width to 13–14 μm, resulting in shading of ≈1.7% of the active cell area. Finally, sintering was performed at 300 °C in forming gas for 10 min.

All lifetime samples were etched back to remove masks and diffused layers using HF dip and TMAH etch. For the lifetime measurements, the samples were passivated with SiN_x layers using PECVD. Carrier lifetimes were measured using the quasi-steady-state photoconductance and transient photoconductance decay techniques with a WCT-120 tool from Sinton Instruments.[23] The carrier lifetimes of the UMG wafers were corrected using carrier mobility values for compensated silicon from Schindler's mobility model.[24] Photoluminescence (PL) images were captured using an LIS-R1 PL imaging tool from BT imaging.[25]

To measure the recombination current densities (J_0), 100 Ω cm n-type FZ control wafers with symmetrical surface structures were used, for both the front-side diffused regions and the rear-side passivating contact. Based on the control samples and Quokka 2[26] simulations, the $J_{0\text{–contacted}}$ and $J_{0\text{–diffused}}$ of 1500 and 52 fA cm^{-2} for the SBD process and 500 and 41 fA cm^{-2} for the DBD process were estimated, respectively. The rear surface, $J_{0\text{–rear}}$, for both processes was 18 fA cm^{-2}.

The illuminated current density–voltage (J–V) and Suns-V_{oc} measurements were performed in-house using an FCT-450 tool from Sinton instruments. The most efficient UMG cell was also independently certified at ISFH CalTeC. Cell reflectance was measured using a Lambda 1050 spectrophotometer from PerkinElmer.

3. Results and Discussion

Figure 1a shows the injection-dependent effective lifetimes for both the UMG-Cz and FZ lifetime samples subjected to both the DBD and SBD solar cell processes, after etching back the diffused layers and repassivating the surfaces. After the TR step, at an injection level of $\Delta n = 1 \times 10^{15}\,cm^{-3}$, the lifetimes of the UMG-Cz wafers increased to 2 ms, which was likely due to the dissolution of lifetime limiting grown-in oxygen precipitate nuclei, as indicated by the increase in $[O_i]$ shown in Figure 1b. After boron diffusion, the effective lifetimes of the UMG-Cz decreased to 360 μs for the SBD process, as shown in Figure 1a. Interestingly, after subsequent phosphorus-doped polycrystalline films deposition, the effective lifetime improved to 670 μs for the SBD process, which highlighted the gettering effect provided by doped-poly films.[16,17]

The implied-open-circuit voltages (i-V_{oc}) measured at 1-sun were derived from the injection-dependent carrier lifetime measurements shown in Figure 1a. The average i-V_{oc} values for the UMG wafers were 630 mV ($\Delta n = 2.3 \times 10^{14}\,cm^{-3}$) and 695 mV ($\Delta n = 2 \times 10^{15}\,cm^{-3}$) for the DBD and SBD processes, respectively. An i-V_{oc} of 630 mV was not sufficient to allow high-efficiency solar cells. Thus, only the SBD process was used to fabricate complete solar cells.

Figure 2 shows the PL images of the UMG wafers subjected to the DBD and SBD processes after all high-temperature steps.

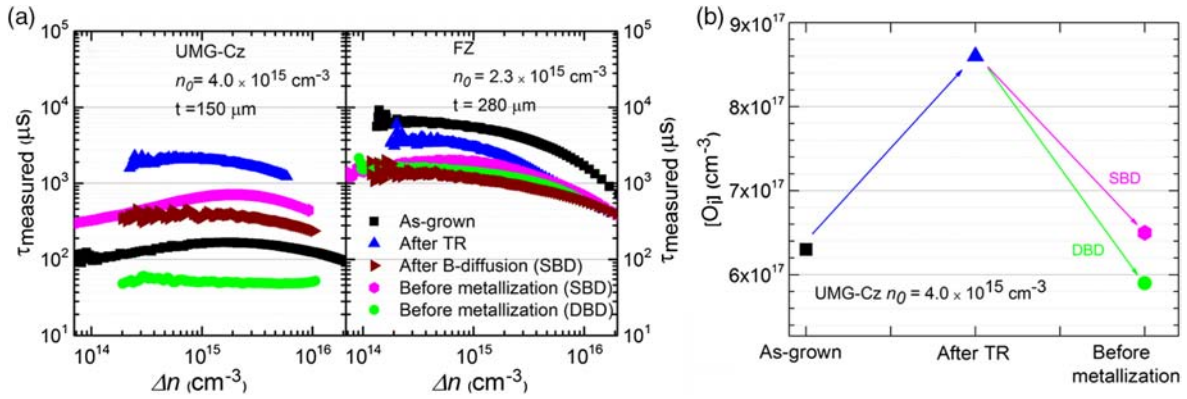

Figure 1. a) Injection-dependent minority carrier lifetimes of planar n-type UMG-Cz and FZ lifetime samples representing as-grown, after TR, after SBD, and after all high-temperature steps (before metallization) for both the SBD and DBD solar cell process, after etch-back and repassivation. b) Average [O_i] present in the UMG-Cz wafers measured by FTIR.

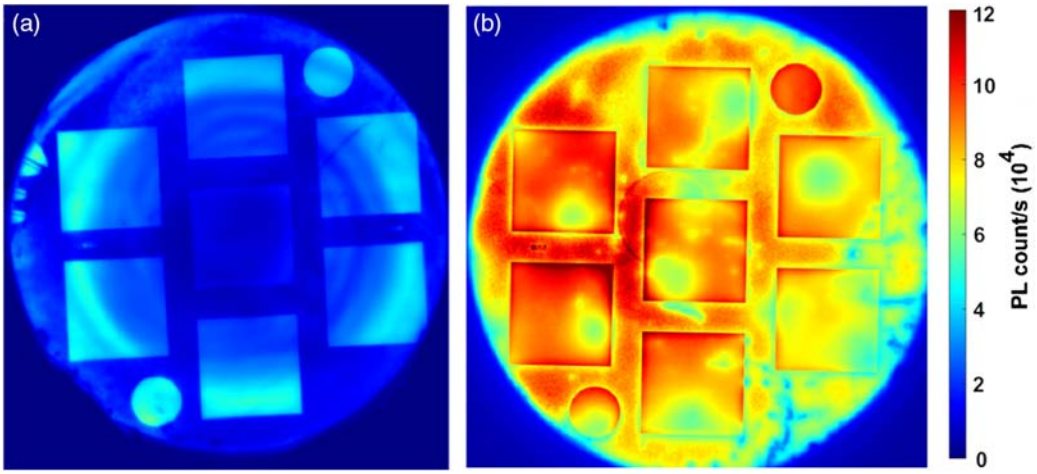

Figure 2. PL images of the 4-inch UMG-Cz cell precursors after all high-temperature steps (before metallization). a) DBD and b) SBD process. PL images were captured at an illumination intensity of 0.5 suns.

Interestingly, we observed ring defects only in the wafers subjected to the DBD process. Note that the nonuniformity on the wafer subjected to the SBD process was due to the front surface passivation. The different thermal responses of the UMG wafers were also reflected in the bulk lifetimes and [O_i], as shown in Figure 1a,b, in which the UMG wafer with the DBD process showed a high degree of bulk degradation and greater losses in [O_i]. The high-thermal budget due to the extra boron diffusion and masking steps in the DBD process caused the renucleation of the oxygen precipitates[27] and/or further growth of the residual oxygen precipitate nuclei which were not fully dissolved during preannealing at 1000 °C,[28] resulting in the appearance of ring defects. Thus, a TR step was not a permanent solution, but provided only a specific window of safe duration at high temperatures, known as the incubation time. The incubation time depended on several factors such as the thermal budget and the initial [O_i], [C], and intrinsic point defects concentrations, all of which affect the reformation of oxygen precipitates in silicon wafers.[27,29,30] Furthermore, a boron diffusion with in situ oxidation do not provide any impurity gettering,[31] therefore requiring a subsequent gettering step to improve the bulk lifetime. Fortunately, the phosphorus-doped polysilicon contacts formed on the rear-side provide such a gettering effect.[16,17]

Table 1 shows the *J*–*V* parameters of the solar cells fabricated in this work. The best UMG cell, certified by ISFH CalTeC, achieved an efficiency of 22.6% and was the highest reported

Table 1. *J*–*V* parameters of the solar cells fabricated in this work.

	V_{oc} [mV]	J_{sc} [mA cm^{-2}]	FF [%]	pFF [%]	η [%]
UMG-Cz (best)	679	40.9	81.1	82.3	22.6
Average (14 cells)	669	40.5	80.5	81.5	22.1
FZ (best)	683	40.7	80.5	83.0	22.4
Average (14 cells)	681	40.6	80.9	82.6	22.2

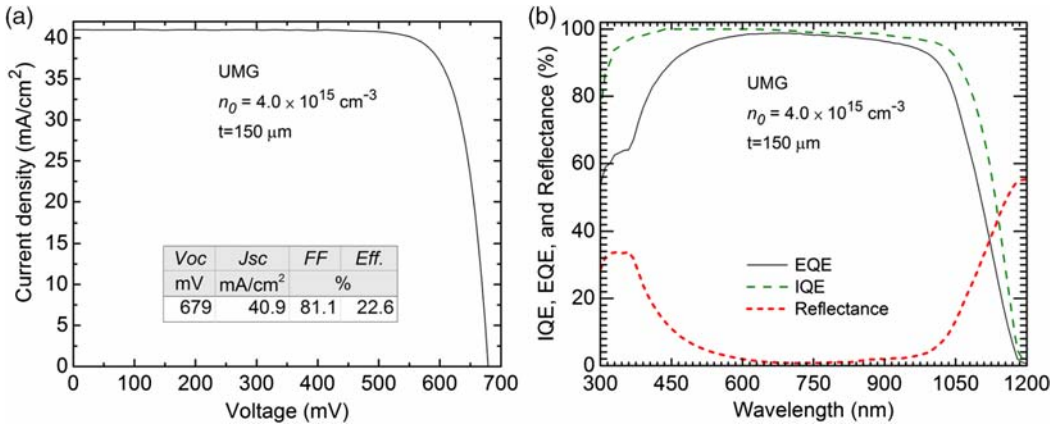

Figure 3. a) Measured *J–V* curve for the champion UMG solar cell with homogeneous boron diffusion. b) Measured EQE, calculated IQE, and measured reflectance curves.

to date for UMG silicon. The *J–V* curve is shown in **Figure 3**a. The best FZ cell demonstrated a very similar efficiency of 22.4%, which is still limited by series resistance as reflected in the difference between FF and pFF, and J_{sc}. However, the V_{oc} is still higher for the FZ cells in comparison with the UMG cells consistent with the effective lifetimes shown in Figure 1a.

Figure 3b shows the measured external quantum efficiency (EQE) and reflectance, and calculated internal quantum efficiency (IQE) curves. The IQE curve for the champion UMG cells shows a very good blue response, even with the SBD.

4. Conclusion

In summary, this work has demonstrated the importance of thermal budget optimization for UMG-Cz wafers. By utilizing a TR step as a prefabrication treatment, selecting a SBD process to minimize the thermal budget, and using full rear-side phosphorus-doped polycrystalline films with excellent impurity-gettering properties as electron-selective contacts, 22.6% efficiency on a cell area of $2 \times 2\,cm^2$ based on n-type UMG-Cz wafers was achieved. This work demonstrates the potential of solar-grade silicon materials to enable high-efficiency solar cells, opening up the possibility of reducing silicon costs by either full or partial substitution of the electronic-grade silicon feedstocks by solar-grade feedstocks.

Acknowledgements

This work was supported by the Australian Renewable Energy Agency (ARENA) through the Australian Centre for Advanced Photovoltaics (ACAP) and projects RND009 and RND017. The ACT node of the Australian National Fabrication Facility is acknowledged for access to their equipment.

Conflict of Interest

The authors declare no conflict of interest.

Keywords

polycrystalline contacts, ring defects, solar-grade silicon, tabula rasa

Received: July 4, 2019
Revised: July 15, 2019
Published online:

[1] J. Kraiem, B. Drevet, F. Cocco, N. Enjalbert, S. Dubois, D. Camel, D. Grosset-Bourbange, D. Pelletier, T. Margaria, R. Einhaus, in *Proc. IEEE Photovolt.* Spec. Conference, **2010**, 1427–1431.
[2] F. E. Rougieux, C. Samundsett, K.C. Fong, A. Fell, P. Zheng, D. Macdonald, J. Degoulange, R. Einhaus, M. Forster, *Prog. Photovoltaics Res. Appl.* **2016**, *24*, 725.
[3] Y. Schiele, S. Wilking, F. Book, T. Wiedenmann, G. Hahn, in *Energy Procedia*, **2013**, *38*, 459–466.
[4] P. Zheng, F. E. Rougieux, X. Zhang, J. Degoulange, E. Einhaus, P. Rivat, D. Macdonald, *IEEE J. Photovoltaics*, **2017**, *7*, 58.
[5] R. Basnet, F. E. Rougieux, C. Sun, S. P. Phang, C. Samundsett, R. Einhaus, J. Degoulange, D. Macdonald, *IEEE J. Photovolt.* **2018**, *8*, 990
[6] R. J. Falster, M. Cornara, D. Gambaro, M. Olmo, M. Pagani, *Solid State Phenom.* **2009**, *57–58*, 123.
[7] V. LaSalvia, A. Youssef, M. A. Jensen, E. E. Looney, W. Nemeth, M. Page, W. Nam, T. Buonassisi, P. Stradins, *Prog. Photovoltaics Res. Appl.* **2019**, *27*, 136.
[8] D. Walter, B. Lim, R. Falster, J. Binns, J. Schmidt, in *Proc. 28th Eur. Photovolt. Sol. Energy Conf. and Exhibition* **2013**, 699–702.
[9] V. Osinniy, A. N. Larsen, E. H. Dahl, E. Enebakk, A. K. Søiland, R. Tronstad, Y. Safir, *Sol. Energy Mater. Sol. Cells*, **2012**, *101*, 123.
[10] A. Peral, J. Manuel Míguez, R. Ordás, C. Del Cañizo, *Sol. Energy Mater. Sol. Cells* **2014**, *130*, 686.
[11] B. Hallam, D. Chen, J. Shi, R. Einhaus, Z. C. Holman, S. Wenham, *Sol. RRL* **2018**, *2*, 1700221.
[12] A. Richter, J. Benick, F. Feldmann, A. Fell, M. Hermle, S. W. Glunz, *Sol. Energy Mater. Sol. Cells* **2017**, *173*, 96.
[13] F. Feldmann, M. Bivour, C. Reichel, H. Steinkemper, M. Hermle, S. W. Glunz, *Sol. Energy Mater. Sol. Cells* **2014**, *131*, 46.
[14] D. Yan, S. P. Phang, Y. Wan, C. Samundsett, D. Macdonald, A. Cuevas, *Sol. Energy Mater. Sol. Cells*, **2019**, *193*, 80.
[15] M. A. Green, *Silicon Solar Cells Advanced Principles and practice*, University of New South Wales, Sydney **1995**.

[16] A. Liu, D. Yan, J. Wong-Leung, L. Li, S. P. Phang, A. Cuevas, D. Macdonald, *ACS Appl. Energy Mater.* **2018**, *1*, 2275.
[17] A. Y. Liu, D. Yan, S. P. Phang, A. Cuevas, D. Macdonald, *Sol. Energy Mater. Sol. Cells* **2018**, *179*, 136.
[18] D. Yan, A. Cuevas, J. Bullock, Y. Wan, C. Samundsett, *Sol. Energy Mater. Sol. Cells* **2015**, *142*, 75.
[19] R. Einhaus, J. Kraiem, S. Martinuzzi, M. C. Record, in *Proc. 21st Eur. Photovolt. Sol. Energy Conf.* **2006**, 580–584.
[20] E. Scheil, *Zeitschrift Met.* **1942**, *34*, 70.
[21] H. Kodera, *Jpn. J. Appl. Phys.* **1963**, *2*, 212.
[22] R. C. Newman, *J. Electrochem. Soc.* **1998**, 257.
[23] R. A. Sinton, A. Cuevas, *Appl. Phys. Lett.* **1996**, *69*, 2510.
[24] F. Schindler, M. C. Schubert, A. Kimmerle, J. Broisch, S. Rein, W. Kwapil, W. Warta, *Sol. Cells* **2012**, *106*, 31.
[25] T. Trupke, R. Bardos, M. Schubert, W. Warta, *Appl. Phys. Lett.* **2006**, *89*, 044107.
[26] A. Fell, *IEEE Trans. Electron Devices* **2013**, *60*, 733.
[27] R. Falster, V. V. Voronkov, *Mater. Sci. Eng. B Solid-State Mater. Adv. Technol.* **2000**, *73*, 87.
[28] E. E. Looney, H. S. Laine, A. Youssef, M. A. Jensen, V. LaSalvia, P. Stradins, T. Buonassis, *Appl. Phys. Lett.* **2017**, *111*, 132102.
[29] S. Zhang, M. Juel, E. J. Vrelid, G. Tranell, *J. Cryst. Growth* **2015**, *411*, 63.
[30] F. Shimura, *J. Appl. Phys.* **1986**, *59*, 3251.
[31] S. P. Phang, W. Liang, B. Wolpensinger, M. A. Kessler, D. MacDonald, *IEEE J. Photovolt.* **2013**, *3*, 261.